Available online at www.banglajol.info

Bangladesh J. Sci. Ind. Res. **50(1)**, 21-28, 2015

BANGLADESH JOURNAL OF SCIENTIFIC AND INDUSTRIAL RESEARCH

E-mail: bjsir07@gmail.com

Synthesis of ZnO nanoparticles by a hybrid electrochemical-thermal method: influence of calcination temperature

F. Hassan[1], M. S. Miran[1], H. A. Simol[1,2], M. A. B. H. Susan[1] and M. Y. A. Mollah[1]*

[1]*Department of Chemistry, University of Dhaka, Dhaka 1000, Bangladesh*
[2]*Centre for Advanced Research in Sciences, University of Dhaka, Dhaka 1000, Bangladesh*

Abstract

ZnO nanoparticles (NPs) with size less than 100 nm were successfully prepared by a hybrid electrochemical-thermal method using metallic zinc and $NaHCO_3$ without the use of any zinc salt, template or surfactant. The NPs were characterized by Fourier transform infra-red (FT-IR) spectroscopy, UV-visible spectroscopy, photoluminescence spectroscopy (PL), thermo-gravimetric analysis (TGA), X-ray diffraction (XRD), scanning electron microscopy (SEM) and energy dispersive X-ray (EDX) spectroscopy. UV-visible spectral analysis indicated that the particle size increased with increasing calcination temperature. The band gap (3.91-3.83 eV) was higher for synthesized ZnO NPs than their bulk counterparts (3.37 eV). The FT-IR spectra at different calcination temperatures showed the characteristic band for ZnO at 450 cm^{-1} to be prominent with increasing temperature due to the conversion of precursor into ZnO. The wurtzite hexagonal phase was confirmed by XRD analyses for ZnO NPs calcined at 700 ^oC. The green photoluminescent emission from ZnO NPs at different calcination temperatures is considered to be originated from the oxygen vacancy or interstitial related defects in ZnO. SEM images clearly showed that the NPs are granular and of almost uniform size when calcined at higher temperatures. EDX spectra further confirmed the elemental composition and purity of ZnO obtained on calcination at 700 ^oC. The NPs are well dispersed near or above calcination temperature of 700 ^oC.

Keywords: ZnO nanoparticles; Semiconductor; Calcination; Particle size; Hybrid-electrochemical-thermal method

Introduction

Zinc oxide (ZnO), due to its excellent semiconducting and gas sensing properties and photocatalytic and antibacterial activities, is an important material for photovoltaic cells (Rensmo *et al.*., 1997; Bauer *et al.*, 2001; Thool *et al.*., 2014), optoelectronic devices (Tennakone *et al.*, 1999; Zhang et al., 2002; Govender *et al.*, 2002) and sensors (Dong *et al.*, 1997; Gupta, 1990; Henning *et al.*, 1990; Chaturvedi *et al.*, 2012). The recent bias has been shifted towards the investigation of ZnO at nano-scale. Development of a suitable low-cost method operable at ambient temperature for the preparation of ZnO nanoparticles with enhanced semiconducting properties along with other properties remains a challenge to the researchers. The growth kinetics of ZnO nanoparticles (NPs) from a basic solution of zinc acetate using different solvents has been investigated to demonstrate that the particle growth and coarsening are strongly dependent on the solvent (Syeeda *et al.*, 2008). Propanol-2 has been found to be the most suitable solvent. The effect of surfactants on the growth kinetics of ZnO NPs in reverse micellar system has also been reported (Ahmed *et al.*, 2013). Moreover, ZnO@Ag core@shell NPs have been prepared by using water-in-oil microemulsions (Satter *et al*. 2014). Particle size determination by effective mass model (EMM) (Holleman *et al.*, 2001; Brus 1986) indicates a uniform particle size distribution of ZnO NPs in reverse micellar solutions; and both anionic, viz. sodium dodecyl sulfate (SDS) and cationic, cetyltrimethylammonium bromide (CTAB) surfactants effectively influences the growth kinetics of ZnO NPs.

Although reverse micellar systems have proved themselves as promising media for preparation of ZnO NPs, isolation of ZnO NPs in the solid state is troublesome and more often limited by coagulation. For large scale preparation of ZnO NPs, the ease of preparation and extraction in the solid state are very important and a novel methodology to prepare ZnO NPs with controllable size, desirable morphology and homogeneous and uniform distribution of particles is critically sought for. In this context, electrochemical methods have gained considerable interest because of their simplicities, low temperature operations, and viabilities for commercial production (Chandrappa *et al.*, 2010; Zhu *et al.*, 2006; Geeetha and Thilagavathi, 2010). The effects of electrolyte concentration and current density on the yield for ZnO NPs have already been reported and the effect of

*Corresponding author: E-mail: myamollah@hotmail.com

calcination temperatures on the morphology and size of ZnO has been touched upon (Chandrappa *et al.*, 2010); but a clear understanding of the effect of calcination temperature on the morphology and size of ZnO still remains an unresolved issue. A systematic approach to thoroughly investigate the growth kinetics of ZnO NPs at different calcination temperatures and tune size and morphology for task-specific applications is yet to be made.

In this study, we report the synthesis of ZnO NPs by an electrochemical-thermal method using metallic zinc as a precursor avoiding the use of any surfactants or template. Particular emphasis has been given on the influence of calcination temperature on the morphology and size of ZnO NPs. The ultimate goal has been to optimize the condition for large scale production of ZnO with controllable size and morphology using the low-cost hybrid method.

Materials and methods

Materials

High purity zinc metal plates (99.99%) were purchased from Sisco Research Laboratories and were cut into pieces of required size and shape for use as electrodes. Sodium bicarbonate (Merck, Germany) and nitric acid (Merck, Germany) were used without any further purification. Ultrapure water (resistivity, ρ =18.0 MΩ cm) used in this study was collected from a water purifier (BOECO pure, model- BOE 8082060, Germany).

Preparation of ZnO NPs

A two-electrode monopolar electrolytic cell (Chandrappa *et al.*, 2010) with zinc as sacrificial anode was used for electrochemical synthesis of ZnO. The electrodes were supported on a holder made of ebonite and placed inside the electrolyte solution comprising 0.009 M $NaHCO_3$. Electrolysis was carried out on average temperature of ca. 30 °C for 1 h by passing fixed amount of current of 2A, following the condition optimized in the literature (Chandrappa *et al.*, 2010). The resulting white precipitates were filtered and air-dried for 12 hours. These were used as precursors and calcined at different temperatures from as low as 60 °C to maximum of 700 °C for 1 hour. The possible chemical reaction scheme is-

$$NaHCO_3(s) + H_2O(l) \leftrightarrow Na^+(aq) + HCO_3^-(aq)$$

$$HCO_3^-(aq) + H_2O(l) \leftrightarrow H_2CO_3(aq) + OH^-(aq)$$

$$Zn(s) \rightarrow Zn^{2+}(aq) + 2e^-$$

$$Zn^{2+}(aq) + 2OH^-(aq) \rightarrow Zn(OH)_2(s)\downarrow$$

$$Zn^{2+}(aq) + 2HCO_3^-(aq) \rightarrow ZnCO_3(s)\downarrow + H_2O(l) + CO_2(g)$$

Upon calcination precursors ($Zn(OH)_2$ and $ZnCO_3$) were converted to ZnO.

Characterization of ZnO NPs

ZnO NPs were characterized to understand the changes of physical and optical properties with calcination temperature. The band gap of the ZnO NPs was calculated from UV-visible (UV-vis) spectrum (Shimadzu 1650) by using EMM (Holleman *et al.*, 2001; Brus, 1986). An FT-IR spectrometer (Shimadzu FT-IR IR-Prestige-21) was used to identify products at different temperatures. Thermogravimetric analysis (TG-DTA 7200, Hitachi, Japan) of the precursor was performed to find out temperature for its conversion to ZnO and to predict the possible chemical changes taking place during calcination. Thermal analysis of about 10 mg of the sample was carried out at a heating rate of 5 °C per min from ambient temperature upto 900 °C in an alumina pan under nitrogen atmosphere. Photoluminescence (PL) spectroscopy (F-7000 FL Spectrophotometer) was used to study the surface defect. An X-ray diffractometer (PAN analytical X' Pert PRO XRD PW 3040; CuK_α radiation) was used to analyze the phase composition. Scanning electron microscopy (SEM) was used for morphological analysis. The stoichiometry of the calcined samples was examined by the energy dispersive X-ray (EDX) spectroscopy. The SEM images and EDX spectra of prepared samples were recorded using a SEM and EDX spectrometer (Hitachi S-3400N, Japan).

Results and discussion

FT-IR spectroscopy

FT-IR spectra of precursor and ZnO NPs calcined at different temperatures (Fig.1) were recorded in the range of 319-4000 cm^{-1}.

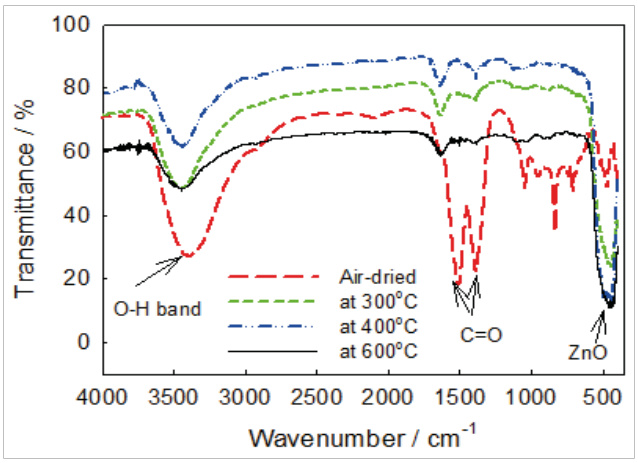

Fig. 1. FT-IR spectra of the precursor and ZnO NPs calcined at different temperatures.

The band at 450 cm^{-1} is characteristic of ZnO (Lili et al., 2006). The absorption bands of air dried sample correspond to $ZnCO_3$ and $Zn(OH)_2$. On heating to 300 °C and higher temperatures, the band at 1500, 1387 and 700-1100 cm^{-1} disappear and a band at 450 cm^{-1} for Zn=O appears. Absorbed water is present in all samples. The stretching modes of vibrations in asymmetric and symmetric C=O vibration bands and bending vibrations of $Zn(OH)_2$ are observed at 1387 and 1500 cm^{-1}. The lattice vibration bands of CO_3^{2-} appear within 700-1100 cm^{-1} due to the lattice vibration of CO_3^{2-} in air dried sample, but is absent in calcined samples (Yongning *et al.*, 1996). Moreover, the band in the range 3200-3600 cm^{-1} is due to intermolecular hydrogen bond due to absorbed water.

Thermogravimetric analysis (TGA)

Fig. 2 shows the TG-DTA patterns for air dried ZnO precursor. The first weight loss in the range of 30-100 °C is due to removal of surface adsorbed water. About 2.41% weight loss within 100-150 °C correspond to the removal of trapped water molecule and desorption of hydroxide ion (Chandrappa *et al.*, 2010). The major weight loss of 17.87% is observed within 150-280 °C for decompositions of $Zn(OH)_2$ and $ZnCO_3$ (Chandrappa *et al.*, 2010). The precursor loses its weight (1.86%) in the temperature range of 300-440 °C, possibly due to the decarbonation process at higher temperature (Vágvölgyi *et al.*, 2008). Although decarbonation is expected to be completed within 280 °C, slower diffusion of CO_2 from the core of particles is slow to exhibit weight loss in this temperature range. Some oxygen loss may occur at higher temperature (Vágvölgyi *et al.*, 2008), which is observed between 440-650°C (weight loss 0.4%).

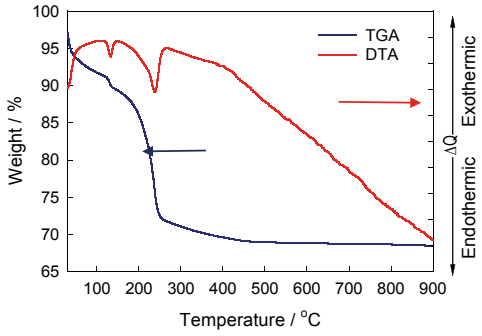

Fig. 2. TG-DTA pattern of ZnO precursor.

There are two endothermic peaks in the DTA curve; one (120-145 °C) corresponds to the evaporation of absorbed and trapped water and another (150-262 °C) corresponds to the simultaneous decomposition of hydroxide and carbonate (Chandrappa et al., 2010). It is concluded that the formation of ZnO takes place on heating to 300 °C; but complete crystallinity is achieved on heating at 700 °C.

UV-Visible spectroscopy

The UV-visible absorption spectra of different samples dispersed in water are shown in Fig. 3. The cut-off wavelength was obtained from the absorption spectra following the procedure described in literature (Hale et al., 2005). The slope at half the peak maximum was estimated and the cut-off wavelength was measured from where the tangent crossed the λ- axis (X-intercept).

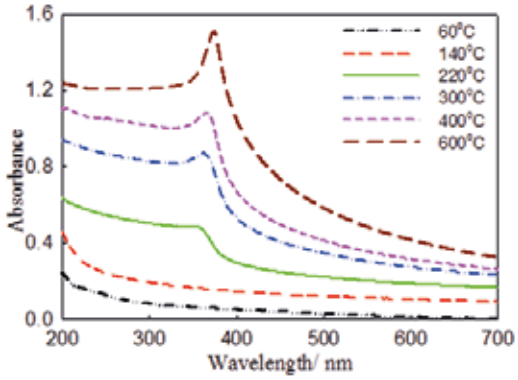

Fig. 3. UV-vis spectra of ZnO NPs calcined at different temperatures.

Table I. Band gap energy of ZnO NPs at different calcination temperatures (from Fig. 3).

Calcination temperature (°C)	Cut-off wavelength (nm)	Band gap energy (eV)
60	----	----
140	---	----
220	407	3.89
300	406	3.88
400	406	3.87
600	407	3.86

Fig. 3 shows that the corresponding absorption band (λ_{max}) remained almost identical (406-407 nm) with change in calcination temperature from 220 to 600 °C. The band gap energy was found in the range of 3.86-3.89 eV and did not show any noticeable change with growth of the NPs on increasing calcination temperature. Particle size estimated from EMM shows the values in the range of 1.52 to 1.55 nm.

Formation of NPs could not be marked between 60 to 140 °C. The ZnO NPs generated via electrochemical method are in blue region compared to the bulk ZnO (3.37 eV) in agreement with the literature data (Chandrappa et al., 2010; Wang et al. 2009). The difference in the band gap is related to the presence of vacancies and dopants (Wang *et al.* 2009).

Photoluminescence emission

Photoluminescence spectra of ZnO NPs at different calcination temperatures are given in Fig. 4. These typically consist of a weak UV emission band (a) and a sharp visible emission band (b) in agreement with literature (Singh *et al.*, 2008). The UV emission band related to a near band-edge transition of ZnO appears at ca. 337 nm. A significant enhancement (ca. 300 times) is observed for the intensity of air-dried sample that partially covers violet-blue region in the visible spectrum. Thus, it is assumed that the blue emission of air-dried sample (Fig. 4 (a) originates from transitions involving zinc interstitial defect structures.

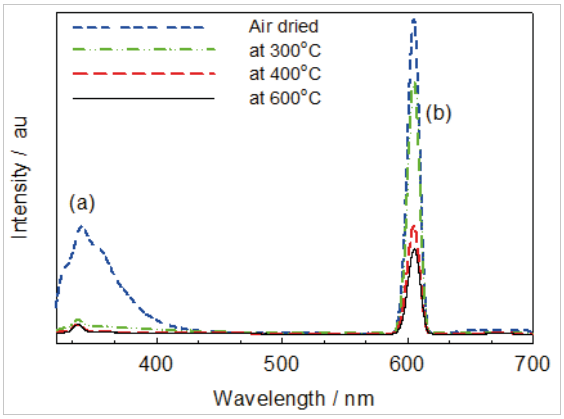

Fig. 4. Photoluminescence spectra of the precursor and ZnO NPs calcined at different temperatures.

A strong and wide PL signal in the range from 590 to 620 nm, with maximum at ca. 605 nm in the yellow-orange range is attributed to oxygen vacancy (Singh *et al.*, 2008; Aguilar *et al.*, 2009). The low temperature-dried sample provides sufficient ionization energy and increases the concentration of charged zinc interstitials, strengthening the blue emissions. The high temperature calcination induces the outward diffusion of zinc interstitials and diminishes the blue emissions. Therefore, the ZnO NPs calcined at higher temperatures do not show the presence of zinc interstitial defect states. In general, the smaller the particle size, the larger is the surface oxygen valence content, the higher is the probability of exciton occurrence, and the stronger is the PL signal (Singh *et al.*, 2008; Aguilar *et al.*, 2009). Furthermore, the PL intensity of ZnO NPs decreases with increasing particle size on increasing calcination temperature to indicate that oxygen vacancy decreases with increasing calcination temperature due to the formation of larger ZnO crystallite at high temperatures. However, the PL peak positions do not change, indicating that there are a few fixed exciton energy levels on the surface of ZnO NPs, which are possibly related to the surface states resulting from the oxygen vacancies and adsorbed oxygen. The results show that the smaller the particle size, the more is the surface oxygen content, and the stronger is the PL signal of ZnO NPs. This is due to the fact that the PL signals result mainly from the oxygen vacancies, which favor the photocatalytic reactions, indicating that the surface oxygen vacancies play an important role in exhibiting the material functional performance.

X-Ray diffraction (XRD) of ZnO NPs

Fig. 5 shows the X-ray diffraction pattern of ZnO calcined at 700 °C. The experimental *d*-values are in close agreement to the JCPDS *d*-values.

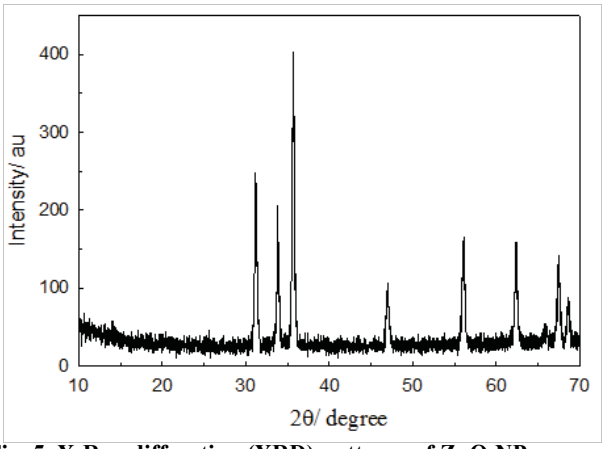

Fig. 5. X-Ray diffraction (XRD) patterns of ZnO NPs prepared from ZnO precursor by calcination at 700 °C.

It suggests that complete crystallinity of ZnO NPs can be achieved on calcining the precursor at 700 °C, which supports the TGA results (*vide supra*). The characteristic XRD peaks with the corresponding intensities detected at 2θ positions are summarized in Table 2. In this case, the experimental *d*-values are in good agreement with the JCPDS *d*-values (Jakuphanoglu *et al.*, 2007; Lupan *et al.*, 2008) and 100 % intensity was observed for (101) plane (hkl) similar to pure ZnO. Complete crystallinity could be achieved after calcining the sample at 700 °C. For the XRD diffractogram of ZnO NPs calcined at 700°C, the crystallite size *D*, was determined using Debye Scherer formula (Geeetha and Thilagavathi, 2010):

$$D = \frac{K\ \lambda}{\beta\ \cos\ \theta} \qquad (1)$$

where K = 0.9, is the shape factor, λ = 1.5408Å, θ is the diffraction peak angle (Bragg angle) in degrees, and β denotes the full width at half maximum (FWHM) in degree, of the corresponding diffraction peak. The crystallite size for (100) plane was found to be 51.59 nm (eq. 1). The lattice parameters for hexagonal ZnO calcined at 700 °C were calculated using equation (2).

$$\frac{1}{d^2} = \frac{4}{3}\left(\frac{h^2 + hk + k^2}{a^2}\right) + \frac{l^2}{c^2} \qquad (2)$$

Lattice parameters of ZnO calcined at 700 °C were determined from eq. 2 as a = 3.27 Å and c = 5.26 Å which are similar to those of JCPDS standard data (a = 3.25 Å and c = 5.21 Å) for pure ZnO. It can be inferred from data presented in Table II. that ZnO NPs prepared by hybrid-electrochemical method possess hexagonal wurtzite phase.

Scanning electron microscopy (SEM)

The SEM images of ZnO NPs obtained at different calcination temperatures are shown in Fig. 6. The shapes of ZnO NPs calcined at 700 °C are granular and almost uniform in size. The mean size of NPs was below 100 nm. This agrees well with the particle size determined by XRD analysis, where the NPs prepared at 700 °C of calcination temperature give average crystallite size of 53 nm.

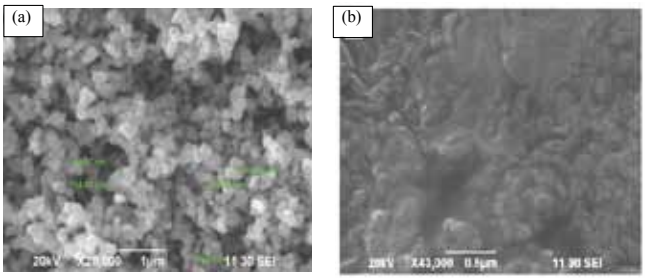

Fig. 6. SEM image of ZnO NPs calcined at (a) 700 °C and (b) 300 °C.

Table II. Characteristic *d*- spacing and 2θ values observed for pure ZnO and ZnO NPs calcined at 700 °C.

Pure ZnO*				Calcined ZnO NPs at 700 °C			
d-spacing	2θ	Intensity	h k l	*d*-spacing	2θ	Intensity	h k l
2.82	31.75	57.65	1 0 0	2.86	31.24	64.44	1 0 0
2.61	34.40	43.66	0 0 2	2.64	33.95	48.55	0 0 2
2.48	36.22	100.00	1 0 1	2.51	35.74	100.00	1 0 1
1.91	46.51	23.28	1 0 2	1.93	47.02	18.45	1 0 2
1.63	56.57	31.82	1 1 0	1.64	56.11	34.89	1 1 0
1.48	62.83	30.21	1 0 3	1.49	62.47	25.58	1 0 3
1.38	67.92	25.53	1 1 2	1.39	67.53	22.17	1 1 2
1.36	69.06	12.97	2 0 1	1.37	68.64	12.87	2 0 1

* Lupan et al., 2008 and Jakuphanglu et al., 2007

To monitor the influence of calcination temperature on the formation of ZnO NPs, SEM image of ZnO NPs calcined at 300 °C was also taken. At lower calcination temperatures, the randomly oriented spindle-like ZnO NPs were observed (Fig. 6(b)). This indicates that calcination temparature plays a crucial role in the morphology of NPs. This also agrees with the TGA analysis that nucleation of crystalline ZnO begins at about 300 °C. This is also in agreement with UV-vis results which show that the higher calcination temperature is a requisite for nucleation of ZnO nanocrystals (Chandrappa *et al.*, 2010).

Energy-dispersive X-ray (EDX) spectroscopy

The stoichiometry of ZnO NPs calcined at 700 °C was examined by the EDX spectrum as shown in Fig. 7. Only signals corresponding to zinc and oxygen have been detected, suggesting that the NPs are indeed made up of Zn and O and no other impurities were present in the samples. This indicates that calcined ZnO NPs is 100 % pure. Composition of elements in ZnO NPs prepared by electrochemical method was such that O was 18.50 % and Zn was 81.50%, which are closer to the calculated values.

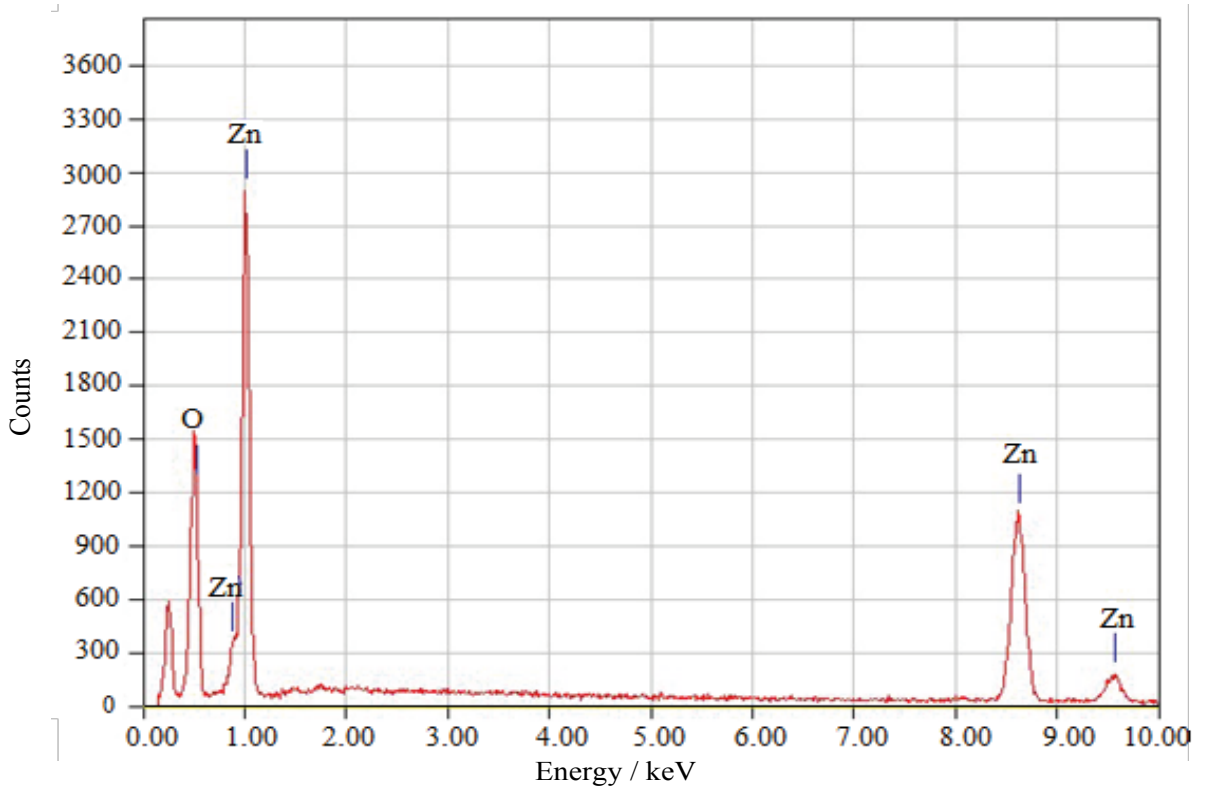

Fig. 7. EDX analysis of ZnO NPs calcined at 700 °C.

Conclusion

ZnO NPs with sizes less than 100 nm were successfully prepared from metallic zinc and $NaHCO_3$ by an electrochemical-thermal method. Analyses of ZnO NPs so prepared have almost uniform morphology when calciniation temperature is near 700 °C or above. Morphology and sizes of ZnO could therefore be controlled by changing calcination temperature. The ambient temperature operation of the electrochemical method together with the ease of separation due to the insolubility of precursor in eletrolytic solution have made the hybrid method so attractive. The method is simple and may, therefore, be effectively used to synthesize ZnO NPs on a large scale at a lower cost.

Acknowledgment

This study was funded under the sub-project, "Development of Novel Functional and Smart Materials for Technological Applications" (CP-231), under Higher Education Quality Enhancement Project (HEQEP) of the University Grants Commission of Bangladesh.

References

Aguilar CA, Haight R, Mavrokefalos A, Korgel BA and Chen S (2009), Probing electronic properties of molecular engineered zinc oxide nanowires with photoelectron spectroscopy, *ACS Nano*. **3:** 3057-3062.

Ahmed P, Miran MS, Susan MABH and Mollah MYA. (2013), Growth process of zinc oxide nanoparticles in presence of reverse micelles of anionic and cationic surfactants, *J. Bangladesh Chem. Soc.* **26**: 60.

Bauer C, Boschloo G, Mukhtar E and Hagfeldt A (2001), Electron Injection and Recombination in $Ru(dcbpy)_2(NCS)_2$ Sensitized Nanostructured ZnO, *J. Phys. Chem. B,* **105**: 5585-5588.

Brus L (1986), Electronic Wavefunction Semiconductor Clusters: Experiment and theory, *J. Phys. Chem.* **90**: 2555-2560.

Chandrappa, KG, Venkatesha TV, Vathsala K and Shivakumara C (2010), A hybrid electrochemical–thermal method for the preparation of large ZnO nanoparticles, *J. Nanopart. Res.* **12**: 2667-2678.

Chaturvedi S, Dave PN and Shah NK (2012), Application of nano-catalyst in new era, *J. Saudi Chem.Soc.* **16**: 307-325.

Dong LF, Cui ZL and Zhang ZK (1997), Gas sensing properties of nano-ZnO prepared by arc plasma method, *Nanostruct. Mater.* **8**: 815-823.

Geeetha D and Thilagavathi, T (2010), Hydrothermal synthesis of nano ZnO structures from CTAB, *Digest J. Nanomater. Biostruct*. **5**: 297.

Govender K, Boyle DS, O'Brien P, Binks D, West D and Coleman D (2002), Room-temperature lasing observed from ZnO nanocolumns grown by aqueous solution deposition, *Adv. Mater.* **14**: 1221-1224.

Gupta TK (1990), Application of ZnO Varistors, *J. Am. Ceram. Soc.* **73**: 1817-1840.

Hale, PS, Maddox, LM, Shapter, JG, Voelcker, NH, Ford, MJ and Waclawik, ER, (2005), Growth kinetics and modeling of ZnO nanoparticles**,** *J. Chem. Edu.*. **82**: 775.

Henning, DFK, Hartung R and Reijnen PJ, (1990), Grain Size Control in Low-Voltage Varistors**,** *J. Am. Ceram. Soc.* **73**: 645-648.

Holleman, AF and Wiberg E (2001), Inorganic Chemistry, Academic Press, San Diego. Houyi, M, Bingsheng Y, Shuyun W, Yongli J, Wei P, Shaoxin H, Shenhao C and Fanjun M (2004), Synthesis of silver and gold nanoparticles by a novel electrochemical method, *Chem. Phys. Chem.* **5:** 68-75.

Jakuphanoglu F, Ilican S, Caglar M, Caglar, Y (2007), The determination of the optical band and optical constants of non-crystalline and crystalline ZnO thin films deposited by spray pyrolysis, *J. Optoelec. Adv. Mat.* **9**: 2180.

Lili W, Youshi W, Yuanchang S and Huiying W (2006), Synthesis of ZnO nanorods and their optical, *Rare Met.* **25:** 68-73.

Lupan O, Chow L, Chai G and Heinrich H (2008), Fabrication and characterization of Zn-ZnO core-shell microspheres from nanorods, *Chem. Phy. Lett.* **465**: 249-253.

Rensmo H, Keis K, Lindstrom H, Solbrand A, Hagfeldt A, Lindquist SE, Wang LN and Muhammed M (1997), High light- to-energy conversion efficiencies for solar cells based on nanostructered ZnO electrodes, *J. Phys. Chem. B,* **101:** 2598-2601.

Satter SS, Hoque M, Rahman MM, Mollah MYA and Susan MABH (2014), An approach towards synthesis and characterization of ZnO@AgCore@shell nanoparticles in water-in-oil microemulsion *RSC Adv.***, 4**:20612.

Singh DP, Singh JAI, Mishr PR, Tiwari RS and Srivastava ON (2008), Synthesis, characterization and application of semiconducting oxide (Cu_2O and ZnO) nanostructures. *Bull. Mater. Sci.,* **31**: 319-325.

Syeeda S, Miran MS, Mollah MYA and Rahman MM (2008), Effects of solvents on the growth kinetics of Zinc Oxide Nanoparticles, *J. Bangladesh Chem. Soc.* **21:** 129.

Tennakone K, Kamura GR, Kottegoda IR and Perera VP (1999), An efficient dye-sensitized photoelectrochemical solar cell made from oxides of tin and zinc, *Chem. Commun.* 15-16.

Thool GS, Singh AK, Singh RS, Gupta A and Susan MABH (2014), Facile synthesis of flat crystal ZnO thin films by solution growth method: A micro-structural investigation, *J. Saudi Chem. Soc.*, **18:** 712-721.

Vágvölgyi V, Hales M, Martens W, Kristóf J, Horváth E and Frost RL (2008), Dynamic and controlled rate thermal analysis of hydrozincite and smithsonite, *J. Therm. Anal. Calor.* **92:** 911-916.

Wang XC, Chen XM and Yang BH (2009), Microstructure and optical properties of polycrystalline ZnO films sputtered under different oxygen flow rates, *J. Alloys Compd.* **488**: 232-337.

Yongning H, Xiaoliang S and Lidun M (1996), Synthesis and characterization of nanocrystalline-sized zinc oxide, *Chin J. Appl. Chem.* **13**(4): 92.

Zhang XT, Liu YC, Zhang LG, Zhang JY, Lu YM, Shen DZ, Xu W, Zhong GZ, Fan XW and Kong XG (2002), Structure and optically pumped lasing from nanocrystalline ZnO thin films prepared by thermal oxidation of ZnS thin films, *J. Appl. Phys.* **92:** 3293-3298.

Zhu H, Yang D, Yu G, Zhang H and Yao K (2006), A simple hydrothermal route for synthesizing SnO_2 quantam dots, *Nanotech.* **17**: 2386.

Received: 20 October 2014; Revised: 03 March 2015;

Accepted: 24 March 2015.